# Phase Behavior of Gradient Copolymers

**Run Jiang, Qinghua Jin, Baohui Li,* and Datong Ding**

*College of Physics, Nankai University, Tianjin 300071, China*

**Robert A. Wickham**[†]

*Department of Physics, St. Francis Xavier University, Antigonish, NS, Canada B2G 2W5*

**An-Chang Shi***

*Department of Physics and Astronomy, McMaster University, Hamilton, ON, Canada L8S 4M1*

*Received February 1, 2008; Revised Manuscript Received May 23, 2008*

ABSTRACT: A multiblock model is developed for the study of the phase behavior of gradient copolymers. The model is able to describe gradient copolymer chains with arbitrary composition profiles. The validity of the multiblock model of gradient copolymers is established by good agreement between RPA (random phase approximation) results for a continuous composition distribution and a multiblock model. The phase behavior of gradient copolymers is examined using self-consistent mean-field theory (SCMFT) for multiblock copolymers. Phase diagrams of gradient copolymer melts with different gradient profiles are constructed by solving the SCMFT equations. It is discovered that the phase behavior depends sensitively on the gradient profiles. In particular, new triple points are observed, and the stability region of phases with curved interfaces shrinks as the gradient profile becomes smooth. For linear gradient copolymers, the lamellar phase is predicted to be the only stable ordered phase.

## Introduction

The development of modern synthetic chemistry techniques has made it possible to sequentially add monomers to polymer chains, leading to the ability to produce block copolymers with well-defined molecular weights, block compositions, and chain architectures.[1,2] These block copolymers are able to self-assemble into various ordered microstructures, which have potential applications in nanotechnology.[3] The simplest block copolymer architecture is the linear AB diblock, consisting of a chain of type A monomers covalently bonded to a chain of type B monomers. For an AB diblock copolymer melt, a variety of equilibrium ordered structures have been observed, including lamellae (L), hexagonal-packed cylinders (H), body-centered cubic spheres (S), and a complex bicontinuous gyroid (G) phase.[2] The morphology is controlled by the composition of the diblock copolymer characterized by the volume fraction of the A blocks, $f_A$, and the degree of segregation between the A and B segments characterized by the product of the degree of polymerization of the polymer chain ($N$) and the effective Flory−Huggins interaction parameter, $\chi$.

Recently, an interesting class of copolymers, the so-called gradient copolymers, have been synthesized by living free radical polymerization techniques, such as atom transfer radical polymerization[4−6] and nitroxide-mediated controlled radical polymerization.[7−9] Recent experimental studies using ring-opening metathesis polymerization allowed a high degree of control over the sequence distribution, and the gradient copolymers with a linear gradient or nonlinear gradient shape can be obtained.[10] For block copolymers, the composition changes discontinuously from one block to another, exhibiting a steplike change at the junction point between the blocks. On the other hand, the gradient copolymers are copolymers in which the average composition of the copolymer varies continuously from one end of the chain to another. As illustrated in Figure 1, composition along the chain varies in different ways for AB diblock and gradient copolymers. It has been shown that the gradient copolymers exhibit intermediate behavior as compared with that of the block copolymers and random copolymers[11] and have potential applications as effective blend compatibilizers during melt processing.[12]

In the past few years, there is a growing number of theoretical studies of the properties and applications of gradient copolymers. For the symmetric cases (with the same overall composition $f_A = 0.5$ but differing in composition distribution), Pakula and Matyjaszewski observed lamellar morphologies using computer simulations.[13] Aksimentiev and Holyst studied the phase properties of gradient copolymer melts within the Landau−Ginzburg model, and different scenarios of the phase transformations were revealed in the gradient copolymer systems.[14] By employing a lattice model, Shull and co-workers used numerical self-consistent-field theory to examine the microphase separation morphology[15] in bulk gradient copolymers and describe the equilibrium interfacial behavior of gradient copolymers in immiscible polymer blends.[16] Pickett also described how the significance of the gradient affects the density of free polymer ends at the surface of gradient copolymer brushes.[17] These studies have led to a good understanding of the physical behavior of gradient copolymers. However, a full phase diagram for gradient copolymers has not been worked out so far.

In this paper, a multiblock model is developed to study the phase behavior of gradient copolymers. Copolymers with a

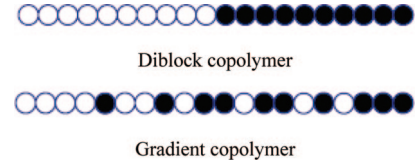


**Figure 1.** Schematic representation of the composition in diblock and gradient copolymers. The open circles denote monomer A, and the closed circles denote monomer B.

* To whom correspondence should be addressed. E-mail: baohui@nankai.edu.cn and shi@mcmaster.ca.

[†] Present address: Department of Physics, University of Guelph, Guelph, ON, Canada N1G 2W1.

10.1021/ma8002517 CCC: $40.75 
Published on Web 06/27/2008

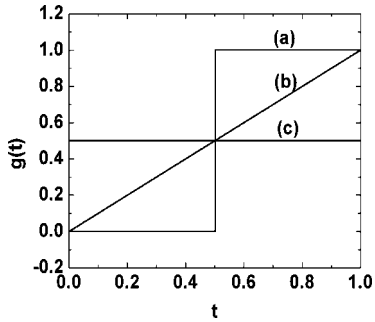


**Figure 2.** Schematic illustration of the composition profile for three copolymers: (a) diblock copolymer, (b) fully linear gradient copolymer, and (c) ideal random copolymer.

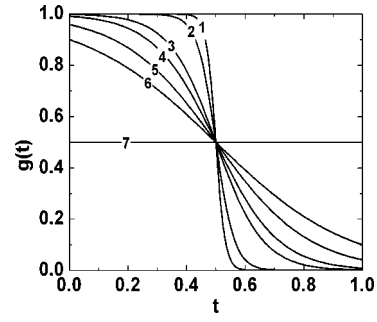


**Figure 3.** Composition profile $g(t) = {}^1/_2[1 - \tanh(C_0\pi(t - t_0))]$ with $t_0 = {}^1/_2$ ($f_A = {}^1/_2$) for various $C_0$. Curve labels correspond to (1) $C_0 = 10$, (2) $C_0 = 5$, (3) $C_0 = 2$, (4) $C_0 = 1.5$, (5) $C_0 = 1$, (6) $C_0 = 0.7$, and (7) $C_0 = 0$.


**Figure 4.** Schematic illustration of the linear multiblock copolymer chain, in which the white and black segments represent A and B blocks, respectively.

continuous gradient distribution function have been studied within the random phase approximation (RPA).[14] While it is straightforward to implement a continuous gradient distribution in real-space SCMFT, it is difficult to implement it in SCMFT formulated in the reciprocal space. On the other hand, reciprocal-space SCMFT is the best tool to obtain accurate phase diagrams. Thus, it is desirable to develop an efficient method to solve the SCMFT of gradient copolymers in reciprocal space. To achieve this goal, a multiblock copolymer chain is used to model gradient copolymers. In what follows we will first define the gradient copolymers and then adopt a multiblock copolymer model to characterize the copolymer with various composition distributions of monomer A and B along the chain. The accuracy of the multiblock model is examined by a comparison with the results from a continuous gradient profile within the RPA theory.[18] Comparison of the spinodal lines of the disordered phase demonstrates that the multiblock approach produces accurate results, thus validating the multiblock model of gradient copolymers. Formulating a self-consistent mean-field theory (SCMFT) for the multiblock model allows us to carry out a systematic study of the phase behavior of gradient copolymer melts with linear and hyperbolic tangent gradient profiles. The results from these calculations are used to elucidate the effects of gradient profile on the phase behavior of gradient copolymers. It is discovered that the phase diagram of gradient copolymers depends sensitively on the gradient profile. As the gradient profile changes from a sharp steplike function (corresponding to block copolymers) to a smooth linear function, the A/B interface becomes diffuse, leading to a larger interfacial width and a weaker degree of segregation. The disorder−order transition point moves to larger $\chi N$. New triple points appear, and these triple points shift to larger $\chi N$, leading to the disappearance of the spherical and gyroidal phases in the parameter range examined.

## Theory

**Continuous Models for Gradient Copolymers.** The architecture of a gradient copolymer can be described by a composition distribution function $g(t)\,dt$,[13] which represents the fraction of A monomers between segment $t$ and segment $t + dt$, in a chain of $N$ segments. Conventionally, $t$ is scaled such that $t \in [0,1]$. The overall composition of A monomers in the copolymer, $f_A$, is the average of $g(t)$ over the chain

$$f_A = \int_0^1 g(t)\,dt \tag{1}$$

Different composition profiles specify different gradient copolymers. All known block copolymers are particular cases of gradient copolymers. We show three examples of composition profiles for gradient copolymers in Figure 2. For a diblock copolymer the gradient profile corresponds to a step function. In this paper, we will study linear gradient copolymers and hyperbolic tangent gradient (or "tanh-gradient") copolymers. For a linear gradient copolymer the profile is a linear function, $g(t) = at + b$, where $a$ and $b$ are constants. In this work we will choose $a = 2f_A$ and $b = 0$, which ensures that

$$g(t) = 2f_A t \tag{2}$$

satisfies eq 1. Since $g(t) \leq 1$, our linear gradient copolymer will only be physically realizable for $f_A \leq 0.5$. Other choices of the constants, such as $a = 2f_A(1 - f_A)$ and $b = f_A^2$, are possible, and such linear gradient copolymers are, in principle, physically realizable for $0 \leq f_A \leq 1$. Such profiles would be interesting for future study since different slope of $g(t)$ might have some effects on the phase behavior.

For the second class of gradient copolymers examined in this work, the tanh-gradient copolymers, the composition profile is specified by

$$g(t) = \frac{1}{2}[1 - \tanh(C_0\pi(t - t_0))] \tag{3}$$

where $C_0$ and $t_0$ are parameters. The composition condition, eq 1, results in a nonlinear relationship between $C_0$, $t_0$, and $f_A$. For $f_A = {}^1/_2$ we have $t_0 = f_A = {}^1/_2$. The parameter $C_0$ controls the width of the transition region from A to B monomers along the chain. The limit $C_0 \to \infty$ corresponds to the steplike composition profile of the diblock copolymer; in this limit $f_A = t_0$. When $C_0 = 0$ in eq 3, we have $g(t) = {}^1/_2$, and this corresponds to a random copolymer with $f_A = {}^1/_2$. For no value of $C_0$ does the tanh-gradient copolymer reduce to the linear gradient copolymer (eq 2). Therefore, these two types of gradient distributions are expected to exhibit different phase behavior. Figure 3 shows the changes in the composition profile for a fixed $t_0 = {}^1/_2$ ($f_A = {}^1/_2$), as $C_0$ decreases. Copolymers with the continuous gradient distribution functions, eqs 2 and 3, have been studied previously using the weak segregation theory.[14]

**Multiblock Model for Gradient Copolymers.** In Figure 4 we introduce a model for a gradient copolymer that partitions the chain into a sequence of $X$ diblock copolymer subchains, which we will call "intervals". The intervals, labeled by $y = 1,..., X$, have their ends positioned at the contour lengths $(y - 1)/X$ and $y/X$; thus, each interval has the same length, $1/X$. We denote the diblock copolymer composition in each interval as $f_A(y)$, and we take $f_A(y)$ to be the average value of the composition profile, $g(t)$, in the interval $y$:

$$f_A(y) = X\int_{(y-1)/X}^{y/X} g(t)\,dt \tag{4}$$

A key advantage of the multiblock model is that, unlike continuous gradient models, it is straightforward to implement the reciprocal-space formulation of SCMFT in this model. In what follows we will examine the multiblock model using both RPA and SCMFT. We mention also that in a realistic scenario of block copolymer synthesis the multiblock construction may be closer to physical reality than the continuous distribution function. Furthermore, we hope that our studies will motivate the synthesis of multiblock copolymers corresponding the to model systems used here.

**Random Phase Approximation for the Structure Factor of the Disordered Phase.** In this subsection we compute the structure factor of the disordered phase within the RPA for both the continuous gradient profile and the multiblock model.[18] A comparison of these two approaches will allow us to test the validity of approximating the continuous gradient profiles using a multiblock model. Details of the RPA analysis are found in refs 18–21. The RPA is based on a Landau-type free energy expansion in powers of the order parameter, $\psi(\mathbf{q})$, where $\psi(\mathbf{q})$ is the Fourier transform of $\psi(\mathbf{r})$, which is the deviation of the microscopic concentration of A monomers from its average value in the disordered phase: $\psi(\mathbf{r}) \equiv \phi_A(\mathbf{r}) - f_A$. The coefficients of the free energy expansion are the vertex functions which are specified in terms of the single-chain correlation functions, $G_{\alpha_1\cdots\alpha_n}(\mathbf{r}_1\cdots\mathbf{r}_n)$.[18–21] The second-order expansion term is proportional to the inverse of the structure factor, $S(\mathbf{q}) = \langle\psi(\mathbf{q})\,\psi(-\mathbf{q})\rangle$. In scattering experiments, $S(\mathbf{q})$ is proportional to the scattering intensity. The inverse structure factor is given by

$$S^{-1}(q) = \frac{\sum_{\alpha,\beta} G_{\alpha\beta}(q)}{\det \mathbf{G}} - 2\chi \tag{5}$$

where $G_{\alpha\beta}$ are the second-order single-chain correlation functions with $\alpha, \beta = (A, B)$ and $\mathbf{G}$ is the matrix formed by the $G_{\alpha\beta}$. For a monodisperse linear copolymer melt the $G_{\alpha\beta}$ have the form

$$G_{\alpha\beta}(q) = N\int_0^1 dt_1\int_0^1 dt_2\, g_\alpha(t_1)\, g_\beta(t_2) e^{-(b^2/6)Nq^2(|t_1-t_2|)} \tag{6}$$

where $g_\alpha(t)$ and $g_\beta(t)$ are the composition profiles of the chains of type $\alpha$ and $\beta$, respectively.

Equation 6 is a general result, which can be applied either to cases of block copolymers or gradient copolymers, depending on the specific form of the gradient profiles.[14] For a general continuous gradient profile, evaluation of $G_{\alpha\beta}$ can be performed numerically. However, for linear gradient copolymers specified by eq 2, the correlation functions can be obtained analytically. With $x \equiv (b^2/6)N\mathbf{q}^2 = \mathbf{q}^2R_g^2$, where $R_g$ is the radius of gyration of a chain with $N$ monomers, the correlation functions of linear gradient copolymers are given by

$$G_{AA} = \frac{8f_A^2N}{x^4}\left(\frac{x^3}{3} - \frac{x^2}{2} - xe^{-x} - e^{-x} + 1\right) \tag{7}$$

$$G_{BB} = \frac{2N(1-2f_A)}{x^2}(x + e^{-x} - 1) + \frac{8f_A^2N}{x^4}\left(\frac{x^3}{3} - \frac{x^2}{2} - xe^{-x} - e^{-x} + 1\right) \tag{8}$$

$$G_{AB} = G_{BA} = \frac{8f_A^2N}{x^4}\left[\frac{x^3}{6}\left(\frac{3}{2f_A} - 2\right) + \frac{x^2}{2}\left(1 - \frac{1}{2f_A}\right) + \frac{x^2}{4f_A}e^{-x} + xe^{-x} + e^{-x} - 1\right] \tag{9}$$

For the special case with $f_A = 0$, the correlation function $G_{BB}$ becomes the familar Debye function, $G_{BB}/N = 2/x^2(x + e^{-x} - 1)$, for a B homopolymer. For the case with $f_A = 0.5$, the results of ref 15 are recovered.

For the multiblock copolymer model shown in Figure 4, the corresponding results for the correlation functions of a general gradient copolymer are

$$G_{AA} = N\sum_{y=1}^{X}\sum_{y'=1}^{X}\int_{(y-1)/X}^{(y-1+f_A(y))/X} dt_1\int_{(y'-1)/X}^{(y'-1+f_A(y'))/X} dt_2\, e^{-x(|t_1-t_2|)} \tag{10}$$

$$G_{BB} = N\sum_{y=1}^{X}\sum_{y'=1}^{X}\int_{(y-1+f_A(y))/X}^{y/X} dt_1\int_{(y'-1+f_A(y'))/X}^{y'/X} dt_2\, e^{-x(|t_1-t_2|)} \tag{11}$$

$$G_{AB} = G_{BA} = N\sum_{y=1}^{X}\sum_{y'=1}^{X}\int_{(y-1)/X}^{(y-1+f_A(y))/X} dt_1\int_{(y'-1+f_A(y'))/X}^{y'/X} dt_2\, e^{-x(|t_1-t_2|)} \tag{12}$$

By substituting the above expressions into eq 5, we obtain the inverse structure factor. For a given wavevector $q$, fluctuations of $\psi(\mathbf{q})$ lead to an increase of the free energy if $S^{-1}(\mathbf{q}) > 0$, whereas $S^{-1}(\mathbf{q}) < 0$ implies that fluctuations reduce the free energy. In the latter case these fluctuations will be enhanced, leading to the formation of a phase-separated structure. Thus, the condition $\min_q S^{-1}(\mathbf{q}) = 0$ determines the disordered phase spinodal. The disordered phase spinodal for the multiblock copolymer model can be compared with that from the continuous composition distribution to test the validity of the multiblock model.

**Self-Consistent Mean-Field Theory for the Multiblock Model.** In this subsection, we present the formulation of SCMFT for the multiblock gradient copolymer model. Several reviews of SCMFT are available in the literature.[22–25] We consider an incompressible copolymer melt of $n_c$ AB linear block copolymer chains with a degree of polymerization $N$. The volume of an A monomer as well as a B monomer is $1/\rho_0$. Thus, the total volume of the system equals $V = n_cN/\rho_0$. The polymer chains are modeled as flexible Gaussian chains described by space curves, $\mathbf{R}_i(t)$, where $\mathbf{R}_i(t)$ denotes the position of the $t$th segment of the $i$th chain. We assume that the gradient copolymer is described by the multiblock model in Figure 4. The function $\sigma_\alpha(t)$, with $\alpha = A$ or B, defines the architecture of the multiblock copolymer and is given by

$$\sigma_A(t) = \begin{cases} 1, & \text{if } (y-1)/X \le t \le (y-1+f_A(y))/X \\ 0, & \text{if } (y-1+f_A(y))/X \le t \le y/X \end{cases} \tag{13}$$

That is, $\sigma_A(t)$ equals 1 if monomer $t$ is type $\alpha$ and is zero otherwise. Note that $\sigma_B(t) = 1 - \sigma_A(t)$. We employ the standard polymer model which is specified by a Flory−Huggins interaction, the incompressibility condition, and Gaussian statistics of polymer chains. The partition function for a multiblock copolymer melt is a functional integral over all space curves representing the polymer chains.[26] Within SCMFT, the free energy functional, $F$, of the system is[27]

$$\frac{F}{n_ck_BT} = \frac{1}{V}\int d\mathbf{r}\{\chi N\phi_A(\mathbf{r})\phi_B(\mathbf{r}) - \sum_\alpha \omega_\alpha(\mathbf{r})\phi_\alpha(\mathbf{r}) - \eta(\mathbf{r})(1 - \sum_\alpha \phi_\alpha(\mathbf{r}))\} - \ln Q_c \tag{14}$$

where $k_B$ is the Boltzmann's constant and $T$ is the temperature. We include the Lagrange multiplier $\eta(\mathbf{r})$ to ensure the incompressibility condition. The partition function $Q_c$ of a single multiblock copolymer subject to the fields $\omega_A(\mathbf{r})$ and $\omega_B(\mathbf{r})$ is

$$Q_c = \frac{1}{V}\int D\mathbf{R}(t)P[\mathbf{R}(t);0,1]\exp[-\int_0^1 \mathrm{d}t\{\sum_\alpha \sigma_\alpha(t)\omega_\alpha(\mathbf{R}(t))\}] \tag{15}$$

Here $P$ is the Gaussian weight distribution function. By minimizing the free energy in eq 14 with respect to $\eta(\mathbf{r})$, $\phi_\alpha(\mathbf{r})$, and $\omega_\alpha(\mathbf{r})$, we arrive at a set of SCMFT equations

$$1 - \sum_\alpha \phi_\alpha(\mathbf{r}) = 0 \tag{16}$$

$$\omega_\alpha(\mathbf{r}) = \chi N\phi_\beta(\mathbf{r}) + \eta(\mathbf{r}) \tag{17}$$

$$\phi_\alpha(\mathbf{r}) = -\frac{V}{Q_c}\frac{\delta Q_c}{\delta \omega_\alpha(\mathbf{r})} \tag{18}$$

It is convenient to rewrite $Q_c$ as $Q_c = (1/V)\int \mathrm{d}\mathbf{r}\ q(\mathbf{r},1)$, where $q(\mathbf{r},t)$ is the end-segment distribution function which represents the partition function of a Gaussian chain in the mean fields, with the $t$th monomer on the chain constrained at a given position $\mathbf{r}$. It is straightforward to show that the end-segment distribution function satisfies a modified diffusion equation with an initial condition $q(\mathbf{r},0) = 1$[28]

$$\frac{\partial}{\partial t}q(\mathbf{r},t) = -H_\alpha q(\mathbf{r},t) \tag{19}$$

where the operator $H_\alpha$ in the coordinate-space representation is

$$H_\alpha = -\frac{b^2N}{6}\nabla^2 + \omega(\mathbf{r},t) \tag{20}$$

Here, we define $\omega(\mathbf{r},t) \equiv \sum_\alpha \omega_\alpha(\mathbf{r})\sigma_\alpha(t)$. It is convenient to introduce a second end-segment distribution function $q^\dagger(\mathbf{r},t)$ which satisfies the modified diffusion equation, eq 19, with the right-hand side multiplied by $-1$ and with a different initial condition: $q^\dagger(\mathbf{r},1) = 1$. With the above definitions of the end-segment distribution functions, the local volume fractions $\phi_\alpha(\mathbf{r})$ becomes

$$\phi_\alpha(\mathbf{r}) = \frac{1}{Q_c}\int_0^1 \mathrm{d}t\ \sigma_\alpha(t)\ q(\mathbf{r},t)\ q^\dagger(\mathbf{r},t) \tag{21}$$

The mean-field free energy is then obtained by inserting the mean-field solution into the free energy expression, eq 14. To obtain the mean-field solutions, the SCMFT equations (eqs 16–18) are solved self-consistently using numerical methods. These equations are reformulated in the reciprocal space of a set of basis functions.[27] If $g(\mathbf{r})$ is a function with a given space-group symmetry, we can expand it in terms of the orthonormal basis functions $f_i(\mathbf{r})$:

$$g(\mathbf{r}) = \sum_i g_i f_i(\mathbf{r}) \tag{22}$$

The $f_i(\mathbf{r})$ are eigenfunctions of the Laplacian operator $\nabla^2$ with appropriate space-group symmetry, i.e., $\nabla^2 f_i(\mathbf{r}) = -\lambda_i/D^2 f_i(\mathbf{r})$. $D$ is the periodicity of the structure. The $g_i$ are the amplitudes of $g$ in this basis. In this spectral representation of the self-consistent-field theory, eq 19 becomes

$$\frac{\partial}{\partial t}q_m(t) = -\sum_\alpha \sum_n H_{\alpha,mn}\sigma_\alpha(t)\ q_n(t) \tag{23}$$

where the matrix $H_\alpha$ is given by

$$H_{\alpha,mn}(t) = \frac{1}{6}Nb^2\lambda_m D^{-2}\delta_{mn} + \sum_i \omega_{\alpha,i}\Gamma_{mni} \tag{24}$$

Here, $\omega_{\alpha,i}$ is the amplitude of the field $\omega_\alpha$ and $\Gamma_{mni} \equiv V^{-1}\int f_m(\mathbf{r})f_n(\mathbf{r})f_i(\mathbf{r})\ \mathrm{d}\mathbf{r}$. With the initial condition, $q_m(0) = \delta_{m1}$, the solution to the set of linear differential equations, eq 23, is

$$q_m(t) = \begin{cases} \sum_i T_{\mathrm{A},mi}\left(t - \frac{y-1}{X}\right)q_i\left(\frac{y-1}{X}\right), & \text{if } (y-1)/X \le t \le (y-1+f_\mathrm{A}(y))/X \\ \sum_j T_{\mathrm{B},mj}\left(t - \frac{y-1+f_\mathrm{A}(y)}{X}\right)q_j\left(\frac{y-1+f_\mathrm{A}(y)}{X}\right), & \text{if } (y-1+f_\mathrm{A}(y))/X \le t \le y/X \end{cases} \tag{25}$$

where $T_\alpha(t) \equiv \exp(-H_\alpha t)$ is referred as a transfer matrix that transfers $q_m(t')$ a distance $t$ along the type $\alpha$ regions of the copolymer.[27] The transfer matrix can be easily evaluated by performing an orthogonal transformation $H_\alpha = U_\alpha\Lambda_\alpha U_\alpha^{-1}$ where the elements of the diagonal matrix $\Lambda_\alpha$ are the eigenvalues of $H_\alpha$ and the respective columns of $U_\alpha$ are the corresponding normalized eigenvectors. Since $H_\alpha$ is symmetric, all the eigenvalues will be real and $U_\alpha^{-1} = U_\alpha^T$. We can then express $T_\alpha(t) = U_\alpha \exp(-\Lambda_\alpha t)U_\alpha^T$, from which it follows that

$$T_{\alpha,ij}(t) = \sum_k U_{\alpha,ik}U_{\alpha,jk}\mathrm{e}^{-\lambda_\alpha^{(k)}t} \tag{26}$$

where $\lambda_\alpha^{(k)}$ denotes the $k$th eigenvalue of the matrix $H_\alpha$. Likewise, $q_m^\dagger(t)$ is solved similarly with a different initial condition, $q_m^\dagger(1) = \delta_{m1}$.

Now the single-chain partition function $Q_c$ is given by $q_1(1)$, and the amplitudes of the local volume fractions $\phi_\alpha(\mathbf{r})$ are

$$\phi_{\mathrm{A},n} = \frac{1}{q_1(1)}\sum_{m,l}\Gamma_{nml}\sum_{y=1}^{X}\int_{(y-1)/X}^{(y-1+f_\mathrm{A}(y))/X}\mathrm{d}t\ q_m(t)\ q_l^\dagger(t)$$

$$\phi_{\mathrm{B},n} = \frac{1}{q_1(1)}\sum_{m,l}\Gamma_{nml}\sum_{y=1}^{X}\int_{(y-1+f_\mathrm{A}(y))/X}^{y/X}\mathrm{d}t\ q_m(t)\ q_l^\dagger(t) \tag{27}$$

By substituting the expressions for $q_m(t)$ and $q_m^\dagger(t)$ (eq 25) into eq 27, the integral over $t$ can be carried out analytically. The amplitudes of the local volume fractions are expressed in terms of the eigenvalues and eigenvectors of the matrices $H_\mathrm{A}$ and $H_\mathrm{B}$,

$$\phi_{\mathrm{A},n} = \frac{1}{q_1(1)}\sum_{m,l}\Gamma_{nml}\sum_{y=1}^{X}\sum_{a,b}q_a\left(\frac{y-1}{X}\right)q_b^\dagger \left(\frac{y-1+f_\mathrm{A}(y)}{X}\right)\sum_{j,k}U_{\mathrm{A},mj}U_{\mathrm{A},aj}U_{\mathrm{A},lk}U_{\mathrm{A},bk}S_{\mathrm{A},jk}(y)$$

$$\phi_{\mathrm{B},n} = \frac{1}{q_1(1)}\sum_{m,l}\Gamma_{nml}\sum_{y=1}^{X}\sum_{a,b}q_a\left(\frac{y-1+f_\mathrm{A}(y)}{X}\right)q_b^\dagger \left(\frac{y}{X}\right)\sum_{j,k}U_{\mathrm{B},mj}U_{\mathrm{B},aj}U_{\mathrm{B},lk}U_{\mathrm{B},bk}S_{\mathrm{B},jk}(y) \tag{28}$$

with

$$S_{\mathrm{A},jk}(y) = \frac{\mathrm{e}^{-\lambda_\mathrm{A}^{(j)}(f_\mathrm{A}(y)/X)} - \mathrm{e}^{-\lambda_\mathrm{A}^{(k)}(f_\mathrm{A}(y)/X)}}{\lambda_\mathrm{A}^{(k)} - \lambda_\mathrm{A}^{(j)}}$$

$$S_{\mathrm{B},jk}(y) = \frac{\mathrm{e}^{-\lambda_\mathrm{B}^{(j)}((1-f_\mathrm{A}(y))/X)} - \mathrm{e}^{-\lambda_\mathrm{B}^{(k)}((1-f_\mathrm{A}(y))/X)}}{\lambda_\mathrm{B}^{(k)} - \lambda_\mathrm{B}^{(j)}} \tag{29}$$

The remaining self-consistent field equations become in the reciprocal space of the basis functions

$$\delta_{1i} = \sum_\alpha \phi_{\alpha,i} \tag{30}$$

$$\omega_{\alpha,i} = \chi N\phi_{\beta,i} + \eta_i \tag{31}$$

We solve the self-consistent-field equations iteratively[29] and calculate the mean-field free energy. For an ordered structure, we must also minimize the free energy with respect to the period $D$. We construct the phase diagram by comparing the free energy densities of different structures and selecting the structure with minimal free energy as the equilibrium state.

## Results and Discussion

We choose to study gradient copolymers with linear (eq 2) and tanh-gradient (eq 3) composition profiles. Before we present

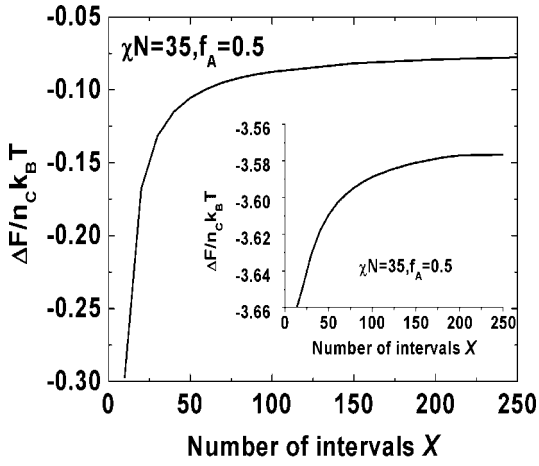


**Figure 5.** Convergence of the free energy, computed within the SCMFT multiblock model, as the number of intervals, $X$, is increased. The main part of the figure is for the lamellar phase of a linear gradient copolymer (eq 2) with $f_A = 0.5$. The result for a tanh-gradient copolymer (eq 3) with $C_0 = 10$ is provided in the inset.

the results of the full self-consistent-field calculations for these gradient copolymer melts, we need to examine the number, $X$, of intervals in the multiblock model which are needed to accurately calculate the free energy of the melt. To this end, we examine the behavior of the free energy density of the lamellar phase $\Delta F/n_c k_B T$, as a function of $X$, for a linear gradient copolymer with $f_A = 0.5$. In Figure 5 we show this free energy, calculated within the SCMFT multiblock model, for $\chi N = 35$. For comparison, we also show the result for a tanh-gradient copolymer with $C_0 = 10$ in the inset of Figure 5.

The free energy density for both the linear and tanh-gradient copolymers increases with the number of intervals, reaching an asymptotic value for large $X$. We expect this since, in the asymptotic limit, the division of the multiblock copolymer into intervals becomes an accurate approximation to a continuous composition profile. We will work in this limit. However, computing with a large number of intervals requires long computation times and large amounts of memory. Therefore, we need to compromise and choose an $X$ that will give us sufficient accuracy at a reasonable computational cost. In what follows we use 200 intervals in our calculation of the phase diagrams. It should be mentioned that the linear gradient copolymers present the worst case in terms of computational accuracy. As shown on the inset of Figure 5, for the tanh-gradient copolymers (eq 3) it is found that using 200 diblocks provides an accurate calculation of the free energy densities.

**Stability of the Disordered Phase.** By comparing the inverse structure factor of the disordered phase, $S^{-1}(q)$, computed exactly using a continuous gradient profile to the $S^{-1}(q)$ obtained using the corresponding multiblock model, we can further test the validity of the multiblock model.

We can also use $S^{-1}(q)$ to calculate the disordered phase spinodal and thereby examine the stability of the disordered phase. For the multiblock model, we will use $X = 200$ in the calculations. In Figure 6 we present the spinodal point, $(\chi N)_s$, as a function of $f_A$ for a linear gradient copolymer melt. For segregations higher than the spinodal, the disordered phase is unstable and ordered structures will form. For the continuous gradient profile with $f_A = 0.5$, we find the critical point occurs at $(\chi N)_c = 29.25$ with a critical period $L_c = 3.41R_g$, which we derive from the critical wavevector $\mathbf{q}_c$ and the expression

$$x_c = q_c^2 R_g^2 = (2\pi/L_c)^2 R_g^2 \tag{32}$$

In the multiblock copolymer model, the critical point occurs at

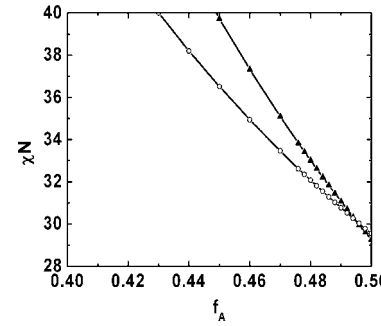


**Figure 6.** Disordered phase spinodal curve for the linear gradient copolymer melt. We calculate the spinodal using a continuous composition distribution (triangles) and also within the multiblock model (circles). The disordered phase is unstable for values of $\chi N$ higher than the spinodal line.

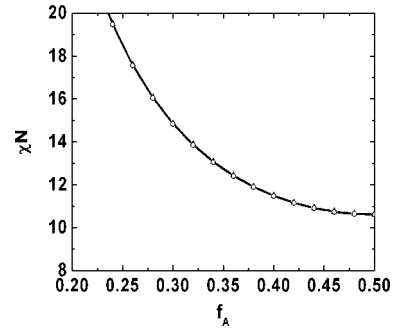


**Figure 7.** Disordered phase spinodal curve for the tanh-gradient copolymer melt with $C_0 = 10$. We calculate the spinodal using a continuous composition distribution (triangles) and also within the multiblock model (circles). The disordered phase is unstable for values of $\chi N$ higher than the spinodal line.

$(\chi N)_c = 29.55$ with $L_c = 3.41R_g$. This demonstrates that the multiblock model gives a reasonably accurate estimate of the critical point, with an error in $(\chi N)_c$ of about 1%. As $f_A$ decreases from 0.5, the disorder spinodal of the multiblock model moves to lower $\chi N$ than the disorder spinodal for the gradient copolymer with a continuous composition, and this deviation becomes progressively worse as $f_A$ decreases. In contrast, for a tanh-gradient copolymer, the multiblock model provides an accurate description of the disorder spinodal over the entire region of the phase diagram we examine in Figure 7. In this case, the critical point occurs at $(\chi N)_c = 10.63$ and $L_c = 3.24R_g$ for the continuous gradient copolymer and at $(\chi N)_c = 10.604$ and $L_c = 3.24R_g$ for the multiblock copolymer model. It should be emphasized that our purpose here is to provide a comparison of the continuous and multiblock composition profiles, not to test the accuracy of the weak segregation theory.

In Figure 8 we examine the spinodal line of the disordered phase for tanh-gradient copolymers with composition profiles corresponding to profiles 1−6 in Figure 3. We employ the multiblock model with $X = 200$. A more gradual composition profile along the copolymer (smaller $C_0$) leads to a higher value for the critical point, and all the spinodal curves lie above that of the diblock copolymer melt.

Figures 9 and 10 show the variation of $(\chi N)_c$ and the critical period (eq 32) with the tanh-gradient profile. The critical period and $(\chi N)_c$ increase sharply when the composition profile varies gradually across the copolymer (i.e., when $C_0$ is small). This is consistent with the fact that an ordered phase does not form in random copolymer melts. The increase in the critical period may arise from stronger chain stretching due to the increase in the critical segregation. In addition, as the composition profile broadens, there is more mixing of A and B monomers at the

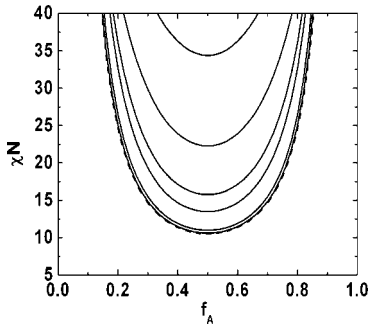


**Figure 8.** Disordered phase spinodal curves for a series of tanh-gradient copolymer melts. From bottom to top, the solid curves correspond to $C_0 = 10$, 5, 2, 1.5, 1, and 0.7. We use a multiblock model with $X = 200$. The dashed curve is the disordered phase spinodal for the diblock copolymer melt.

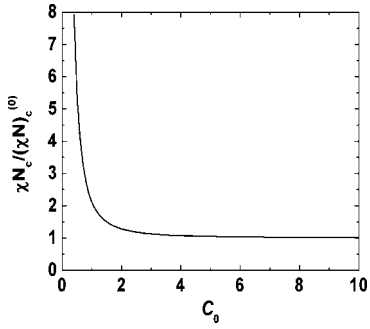


**Figure 9.** Plot of the critical point segregation, $(\chi N)_c$, as a function of the gradient profile, characterized by $C_0$, for a tanh-gradient copolymer melt with $f_A = 0.5$. We use the multiblock model with $X = 200$ to compute the disordered phase structure factor. The critical point segregation is scaled in terms of the critical point segregation for the diblock copolymer, $(\chi N)_c^{(0)} = 10.495$.

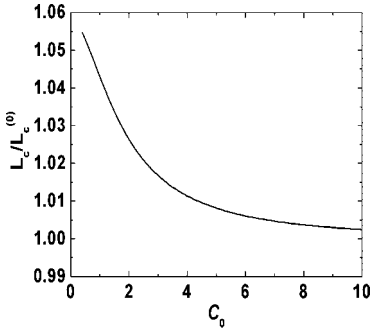


**Figure 10.** Plot of the critical period, $L_c$, as a function of the gradient profile, characterized by $C_0$, for a tanh-gradient copolymer melt with $f_A = 0.5$. We use the multiblock model with $X = 200$ to compute the disordered phase structure factor. The critical period is scaled in terms of the critical period for the diblock copolymer, $L_c^{(0)} = 3.23R_g$.

AB interface, raising the AB interfacial free energy. This would also tend to produce longer periods, as the system attempts to reduce the amount of AB interface. As one would expect, when the profile becomes more steplike (large $C_0$), the critical period and $(\chi N)_c$ approach the values for a diblock copolymer melt, namely, $(\chi N)_c^{(0)} = 10.495$ and $L_c^{(0)} = 3.23R_g$.[18]

**Phase Diagrams.** We construct phase diagrams for gradient copolymer melts by solving the SCMFT equations for the multiblock copolymer model ($X = 200$) with given gradient profiles. Consistent with previous studies of the phase behavior of diblock copolymer melts, we examine the relative stability of four ordered structures (lamellae, hexagonally packed cylinders, bcc spheres, and gyroid) and a disordered phase. It is possible (and would be more interesting) that ordered

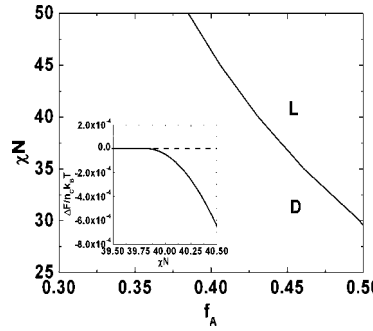


**Figure 11.** Phase diagram for a linear gradient copolymer melt (eq 2). The phase diagram is computed within multiblock SCMFT. The disordered phase is labeled D, and L represents the lamellar phase. The inset shows the behavior of the free energy as a function of $\chi N$ for $f_A = 0.431$ and demonstrates a direct continuous phase transition from D to L.

structures other than these usual candidates may appear in gradient copolymers. However, our main goals in the current paper are to establish the validity of the multiblock model for gradient copolymers and to examine the change in the phase boundaries due to different gradient profiles. Therefore, we leave the possibility of novel phases in gradient copolymers to future study.

We present the phase diagram for the linear gradient copolymer melt (eq 2) in Figure 11. It is interesting that only one ordered structure, the lamellar phase, is present, for the range of $\chi N$ examined. The linear gradient copolymer melt exhibits a direct continuous transition from the disordered to the lamellar phase for all $f_A$ examined. The continuous nature of the transition is evident from the behavior of the free energy curve for the lamellar phase, which is shown for $f_A = 0.431$ in the inset of Figure 11. The minimum in the line of critical points occurs at $(\chi N)_c = 29.55$ and $f_A = {}^1/_2$ for the linear gradient copolymer melt, which is approximately 3 times higher than the value of $(\chi N)_c = 10.495$ for a symmetric, neat diblock copolymer melt. These SCMFT results are consistent with the results from a previous theoretical study of a linear gradient copolymer melt.[14] The observation of a continuous disorder-to-lamellar transition for $f_A \neq 0.5$ is surprising since one expect that in this case the third-order term is not zero by symmetry, and it is well-known that third-order terms in the free energy would lead to a first order transition. However, when the transition is to a lamellar phase, the third-order term is not present. The reason is that, near the transition point, we expect that the density profile be described by the first-mode in Fourier expansion. Since there are no triplets of the first-mode lamellar reciprocal lattice vectors that sum to zero, the third-order term must vanish, leading to a continuous disorder-to-lamellar transition.

In Figure 12 we show the monomer density profiles obtained from multiblock SCMFT for a linear gradient copolymer and a diblock copolymer, both with $f_A = 0.5$. For the diblock copolymer, the degree of segregation of the lamellar domains increases as $\chi N$ is increased, resulting in sharper interfaces. In contrast, for the linear gradient copolymer, the density profile remains sinusoidal-like even for very large $\chi N$. The linear distribution of A and B monomers across a chain leads to a large interfacial width. Diffuse interfaces in gradient copolymers have been noticed previously by Shull.[16]

In Figure 13 we show phase diagrams for the tanh-gradient copolymers (eq 3), computed using the multiblock SCMFT formulated in the reciprocal space. The values of $C_0$ used in the calculations correspond to profiles 1−6 in Figure 3. For comparison, the phase diagram for a neat diblock copolymer melt, computed using SCMFT, is shown in Figure 14. As $C_0$ decreases, the gradient copolymer profile evolves away from

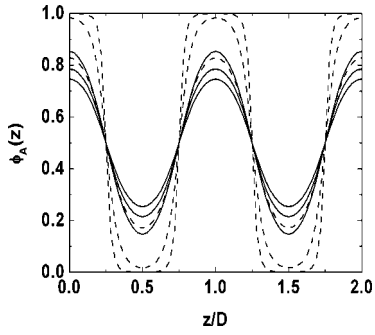


**Figure 12.** Density profile for A monomers in the lamellar structure at $f_A = 0.5$. The solid lines are the multiblock SCMFT results for a linear gradient copolymer melt (at $z = 0$, from bottom to top, the profiles correspond to $\chi N = 40$, 50, and 140). The dashed lines are the SCMFT results for a diblock copolymer melt (at $z = 0$, from bottom to top, the profiles correspond to $\chi N = 12$, 20, and 50). The period of the lamellar structure is $D$.

the sharp interface characterizing the diblock copolymers. The modifications to the diblock copolymer phase diagram begin in the weak segregation region, near $f_A = 0.5$, and spread to higher segregation with decreasing $C_0$. One new triple point appears in the phase diagram (Figures 13a−e). The new triple point indicates the coexistence of the disordered, spherical, and cylindrical phases. The triple points move to smaller values of $f_A$ as $C_0$ decreases. All the phase transition lines in Figure 13 are first-order transitions. This behavior is distinct from that of the linear gradient copolymer, where a direct second-order, transition from the disordered phase to lamellar phase is observed. Thus, our results highlight an important difference between the linear gradient copolymer and the tanh-gradient copolymer. With decreasing $C_0$, the value of $\chi N$ at the critical point increases, and the ODT boundary moves to higher $\chi N$. This behavior is consistent with our weak segregation stability analysis and also with the results of previous studies.[14]

Eventually, with decreasing $C_0$, the sphere and gyroid phases disappear in the region of the phase diagram examined in Figure 13f. Although it is possible that these phases exist at higher values of $\chi N$, we expect that if $C_0$ is small enough, these phases will be completely displaced. The phase boundary depends sensitively on the composition profile. For example, decreasing $C_0$ from 1.5 (Figure 13d) to 1.0 (Figure 13e) leads to a large shift of the phase boundaries, although the composition profile does not change significantly (profiles 4 and 5 in Figure 3). One noticeable difference between these two gradient profiles is that distribution 5 ($C_0 = 1.0$) in Figure 3 does not approach 1 (or 0) at the end points of the polymer, suggesting that this polymer is not able to form strongly segregated domains. We comment below on the implications of diffuse AB interfaces, and weakly segregated domains, for the existence of nonlamellar phases. The disappearance of the spherical phase also occurs as a result of a slight change in the composition profile.

Two factors, which become more important as the AB interface becomes more diffuse, explain the trends seen in Figure 13. First, the observation (Figure 12) that gradient copolymer melts remain relatively poorly segregated, even at high $\chi N$, suggests that phase points occurring at large $\chi N$ in the gradient copolymer phase diagram can be associated with phase points occurring at weaker segregation in the diblock copolymer phase diagram. This explains the shift to higher $\chi N$ of the spinodal, ODT, and all the phase boundaries in the gradient copolymer phase diagram, relative to the diblock copolymer phase diagram. Second, the diffuse nature of the AB interface for the gradient copolymer may reduce the spontaneous curvature of the interface, accounting for the observation that sphere and gyroid phases are eliminated from the phase diagram in order of decreasing average AB interfacial curvature. One can think of the AB interface as a thick layer of almost disordered phase (see the schematic diagram, Figure 15). The disordered layer will have no tendency to curve, so the only tendency to curve will come from the remaining blocks outside this layer. These remaining blocks should have only a weak tendency to curve, compared to blocks in the diblock copolymer, and this will lead to lower values of the spontaneous curvature. Domains with high curvature, such as spheres, would be most sensitive to the reduction in spontaneous curvature in the gradient copolymer and would be eliminated. The reduction of the spontaneous curvature corresponds to associating phase points in the gradient copolymer phase diagram with phase points in the diblock copolymer phase diagram having $f_A$ values closer to 0.5. Taken together with the shift in the phase boundaries to higher $\chi N$, this means that phase points in the gradient copolymer phase diagram can be associated with phase points in the diblock copolymer phase diagram at weaker segregation and closer to symmetric composition. This explains the formation of new triple points and explains why the sphere and gyroid phases march off to the edges of our gradient copolymer phase diagram as $C_0$ is decreased.

The sequence D → S → H → G → L of phase transitions with increasing $\chi N$ that we observe in Figure 13a for $f_A < 0.39$ was seen in a previous theoretical study of the tanh-gradient copolymer, based on a Ginzburg−Landau model.[14] Furthermore, in the nearly symmetric melt, we have observed the D → S → H → L transition sequence which was seen in ref 14. On the other hand, the appearance of a new triple point in Figures 13a−e allows for a new sequence of the phase transitions with increasing $\chi N$: D → H → L, which is not predicted previously. These differences could be attributed to the expansion of the Landau−Ginzburg free energy and the second harmonic approximation imposed by the Landau−Ginzburg theory. Thus, our present SCMFT study is a necessary complement to previous theoretical studies.

## Conclusions

In this paper a multiblock model is used to model the phase behavior of gradient copolymers. Specifically, each gradient copolymer is divided into $X$ subchains, and each subchain is assumed to be an A/B diblock copolymer whose block composition is determined by the gradient copolymer composition profile. We have calculated the spinodal lines of the disordered phase for the gradient copolymer melts in RPA by using two approaches: the continuous gradient profile and the multiblock model. Good agreement is found between the results from these two approaches. It suggests that the multiblock model is a valid model for the studies of the phase behavior of gradient copolymers.

Furthermore, the SCMFT is developed within the multiblock model system, which allows us to go beyond RPA and construct full mean-field phase diagrams over a wide range of segregations for the gradient copolymers melts. We have examined the relative stability of four ordered structures (lamellae, hexagonally packed cylinders, bcc spheres, and gyroid) and a disordered phase for two systems: the linear gradient copolymer and the tanh-gradient copolymer melts.

For the case of the linear gradient copolymer melts, only one ordered structure, the lamellar phase, is found to be stable. In this case, all melts exhibit the direct continuous transition from disordered to the lamellar phase. A diffuse boundary between the domains of A and B is found and causes a larger period of the lamellar structure than in the diblock copolymer melts. This behavior is consistent with the result from previous studies.[14,16]

For the case of tanh-gradient copolymer melts, a small deviation of the composition distribution away from a step

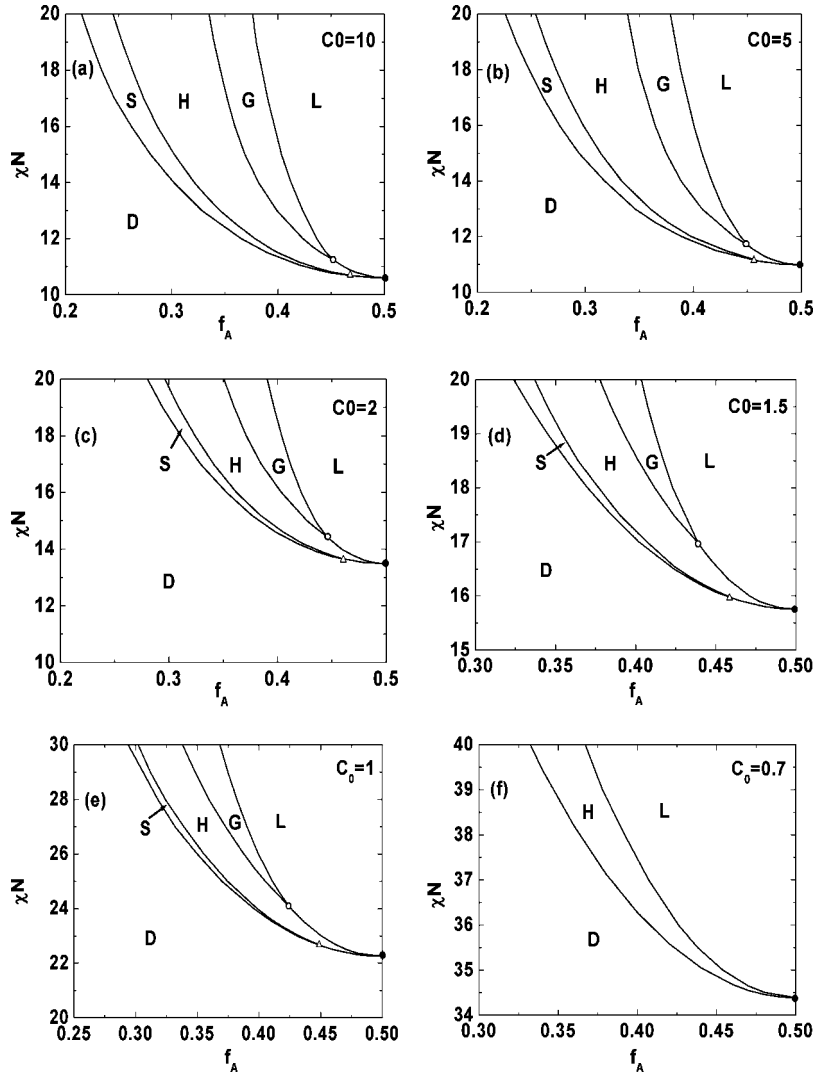


**Figure 13.** Phase diagrams for the tanh-gradient copolymer melts (eq 3), calculated within multiblock SCMFT. (a) $C_0 = 10$, (b) $C_0 = 5$, (c) $C_0 = 2$, (d) $C_0 = 1.5$, (e) $C_0 = 1$, and (f) $C_0 = 0.7$. These values correspond to the composition curves in Figure 3. Here, we observe the disordered phase (D), the lamellar phase (L), the hexagonally coordinated cylinder phase (H), the bcc-spherical phase (S), and the gyroid phase (G). The closed circles, open circles, and open triangles indicate the critical point, H−G−L triple point, and D−S−H triple point respectively.

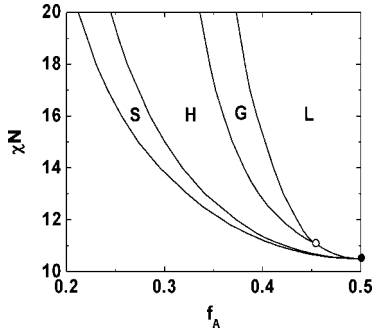


**Figure 14.** Phase diagram of a neat diblock copolymer melt, calculated within SCMFT. The closed circle and the open circle indicate the critical point and the H−G−L triple point, respectively.

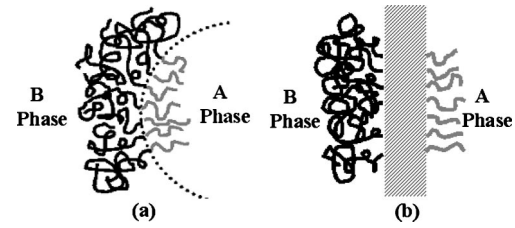


**Figure 15.** Schematic illustration of the mechanism for generating spontaneous curvature in (a) the diblock copolymer interface and (b) the gradient copolymer interface. In (a), the dotted line represents a sharp interface between the A and B phases. In (b), the diffuse interface is shaded.

function cause one new triple point (D−S−H) to appear in the phase diagram. Three scenarios of phase transformations sequences are observed in our systems. The first one corresponds to the transitions from the disorder phase to spherical phase, next to the hexagonal phase, then to the gyroid phase, and finally from the gyroid phase to the lamellar phase. The second scenario of the phase transformation takes place in the following order: from the disorder phase to spherical phases, then to the hexagonal phase, and finally to the lamellar phase. The third scenario of the phase transformation follows the sequence from disordered to the hexagonal phase, then to the lamellar phase.

**Acknowledgment.** This research was supported by the National Natural Science Foundation of China (Grant Nos. 20474034 and 20774052), by the Chinese Ministry of Education with the Program of the Joint-Research Foundation of the Nankai and Tianjin Universities and the Program of New Century

Excellent Talents in Universities (Grants No. ncet–05–0221), and by Nankai University ISC. A.C.S. and R.A.W. acknowledge the support by the Natural Science and Engineering Council (NSERC) of Canada. Both A.C.S. and R.A.W. gratefully acknowledge the hospitality of Baohui Li and Nankai University, where this work was initiated, and St. Francis Xavier University, where the later stages of the manuscript were edited, under a James Chair Visiting Professor Grant.

## References and Notes

(1) Bates, F. S.; Fredrickson, G. H. *Phys. Today* **1999**, *52*, 32.
(2) Hamley, I. W. *Physics of Block Copolymers*; Oxford University Press: Oxford, England, 1998.
(3) Park, C.; Yoon, J.; Thomas, E. L. *Polymer* **2003**, *44*, 6725.
(4) Matyjaszewski, K.; Ziegler, M. J.; Arehart, S. V.; Greszta, D.; Pakula, T. *J. Phys. Org. Chem.* **2000**, *13*, 775.
(5) Matyjaszewski, K.; Xia, J. *Chem. Rev.* **2001**, *101*, 2921.
(6) Davis, K. A.; Matyjaszewski, K. *Adv. Polym. Sci.* **2002**, *159*, 2.
(7) Gray, M.; Zhou, H.; Nguyen, S. T.; Torkelson, J. M. *Macromolecules* **2004**, *37*, 5586.
(8) Gray, M.; Zhou, H.; Nguyen, S. T.; Torkelson, J. M. *Polymer* **2004**, *45*, 4777.
(9) Mignard, E.; Leblanc, T.; Bertin, D.; Guerret, O.; Reed, W. F. *Macromolecules* **2004**, *37*, 966.
(10) Dettmer, C. M.; Gray, M. K.; Torkelson, J. M.; Nguten, S. T. *Macromolecules* **2004**, *37*, 5504.
(11) Lefebvre, M. D.; Dettmer, C. M.; McSwain, R. L.; Xu, C.; Davila, J. R.; Composto, R. J.; Nguyen, S. T.; Shull, K. R. *Macromolecules* **2005**, *38*, 10494.
(12) Kim, J.; Gray, M. K.; Zhou, H. Y.; Nguyen, S. T.; Torkelson, J. M. *Macromolecules* **2005**, *38*, 1037.
(13) Pakula, T.; Matyjaszewski, K. *Macromol. Theory Simul.* **1996**, *5*, 987.
(14) Aksimentiev, A.; Holyst, R. J. *Chem. Phys.* **1999**, *111*, 2329.
(15) Lefebvre, M. D.; Olvera de la Cruz, M.; Shull, K. R. *Macromolecules* **2004**, *37*, 1118.
(16) Shull, K. R. *Macromolecules* **2002**, *35*, 8631.
(17) Pickett, G. T. J. *Chem. Phys.* **2003**, *118*, 3898.
(18) Leibler, L. *Macromolecules* **1980**, *13*, 1602.
(19) Holyst, R.; Vilgis, T. A. *Macromol. Theory Simul.* **1996**, *5*, 573.
(20) Slot, J. J. M.; Angerman, J.; ten Brinke, G. *J. Chem. Phys.* **1998**, *109*, 8677.
(21) Nap, R.; ten Brinke, G. *Macromolecules* **2002**, *35*, 952.
(22) Schmid, F. *J. Phys.: Condens. Matter* **1998**, *10*, 8105.
(23) Matsen, M. W. *J. Phys.: Condens. Matter* **2002**, *14*, R21.
(24) Fredrickson, G.; Ganesan, V.; Drolet, F. *Macromolecules* **2002**, *35*, 16.
(25) Shi, A.-C. In *Developments in Block Copolymer Science and Technology*; Hamley, I., Ed.; John Wiley & Sons: New York, 2004; p 265.
(26) Hong, K. M.; Noolandi, J. *Macromolecules* **1981**, *14*, 727.
(27) Matsen, M. W.; Schick, M. *Phys. Rev. Lett.* **1994**, *72*, 2660.
(28) Helfand, E. *J. Chem. Phys.* **1975**, *62*, 999.
(29) Laradji, M.; Shi, A.-C.; Noolandi, J.; Desai, R. *Macromolecules* **1997**, *30*, 3242.

MA8002517